Journal of Computational Physics 439 (2021) 110405

Contents lists available at ScienceDirect

Journal of Computational Physics

www.elsevier.com/locate/jcp

Maximum bound principle preserving integrating factor Runge–Kutta methods for semilinear parabolic equations

Lili Ju [a], Xiao Li [b], Zhonghua Qiao [b,*], Jiang Yang [c]

[a] Department of Mathematics, University of South Carolina, Columbia, SC 29208, USA
[b] Department of Applied Mathematics, The Hong Kong Polytechnic University, Hung Hom, Kowloon, Hong Kong
[c] Department of Mathematics & SUSTech International Center for Mathematics, Southern University of Science and Technology, Shenzhen 518055, China

ARTICLE INFO

Article history:
Available online 5 May 2021

Keywords:
Maximum bound principle
Integrating factor Runge–Kutta method
Semilinear parabolic equation
High-order numerical methods
Allen–Cahn equations

ABSTRACT

A large class of semilinear parabolic equations satisfy the maximum bound principle (MBP) in the sense that the time-dependent solution preserves for any time a uniform pointwise bound imposed by its initial and boundary conditions. The MBP plays a crucial role in understanding the physical meaning and the wellposedness of the mathematical model. Investigation on numerical algorithms with preservation of the MBP has attracted increasingly attentions in recent years, especially for the temporal discretizations, since the violation of MBP may lead to nonphysical solutions or even blow-ups of the algorithms. In this paper, we study high-order MBP-preserving time integration schemes by means of the integrating factor Runge–Kutta (IFRK) method. Beginning with the space-discrete system of semilinear parabolic equations, we present the IFRK method in general form and derive the sufficient conditions for the method to preserve the MBP. In particular, we show that the classic four-stage, fourth-order IFRK scheme is MBP preserving for some typical semilinear systems although not strong stability preserving, which can be instantly applied to the Allen–Cahn type of equations. To our best knowledge, this is the first time to present a fourth-order linear numerical method preserving the MBP. In addition, convergence of these numerical schemes is proved theoretically and verified numerically, as well as their efficiency by simulations of 2D and 3D long-time evolutional behaviors. Numerical experiments are also carried out for a model which is not a typical gradient flow as the Allen–Cahn type of equations.

1. Introduction

In this paper, we aim to study high-order time discretization methods to preserve the maximum bound principle (MBP) of a class of semilinear parabolic equations taking the following form

$$u_t = \mathcal{L}u + \mathcal{N}[u], \tag{1}$$

where $\mathcal{L}$ and $\mathcal{N}$ are linear and nonlinear operators, respectively, and $u = u(t, \boldsymbol{x})$ is the unknown function subject to appropriate initial and boundary conditions. The MBP implies the existence of special upper and lower solutions in the sense that

* Corresponding author.
E-mail addresses: ju@math.sc.edu (L. Ju), xiao1li@polyu.edu.hk (X. Li), zhonghua.qiao@polyu.edu.hk (Z. Qiao), yangj7@sustech.edu.cn (J. Yang).

https://doi.org/10.1016/j.jcp.2021.110405
0021-9991/

the solution $u(t,x)$ preserves for any time a uniform pointwise bound imposed by the initial and boundary data. Mathematical models for many practical problems have the form (1) and their solutions satisfy the MBP. A typical example is the classic Allen–Cahn equation, where the linear operator $\mathcal{L}$ is the standard Laplace operator multiplied by a diffusion coefficient ε^2 and the nonlinear part is given by a cubic polynomial $\mathcal{N}[u] = u - u^3$. It is well known [16] that the solution to the Allen–Cahn equation is pointwisely bounded by 1 in absolute value for any time if the initial and boundary conditions are bounded by 1, which implies the MBP. The Allen–Cahn equation was originally developed in [2] to model the motion of anti-phase boundaries in crystalline solids, and nowadays, has been widely used as a fundamental model for phase-field (or diffuse-interface) methods to study the interfacial motions and phase transitions in various application fields.

The MBP is an important physical feature and is essential for numerical simulations to yield physically relevant solutions to many mathematical models. Besides the solution to the Allen–Cahn equation, the density, concentration, or pressure in fluid flows must be nonnegative, and the probability distribution should also be in the range $[0, 1]$. Hence, in numerical simulations, it is highly expected that the numerical solutions preserve the MBP in the discrete sense. The violation of MBP may cause the ill-posedness of the problem and blow-ups of the numerical algorithms. For instance, when there is a logarithmic term in the equation, e.g., the reaction-diffusion equation with the Flory–Huggins potential function and the Peng–Robinson equation of state [31,32], a widely used realistic equation of state for hydrocarbon fluid in the petroleum industry, completely wrong results may be obtained if the MBP fails to be preserved, see Section 4.2 for a numerical example. On the other hand, in the view of numerical analysis, the MBP suggests a type of strong stability in the supremum-norm sense and guarantees the spatially uniform pointwise boundedness of the numerical solution. Such a property facilitates the further numerical analysis of the numerical schemes, e.g., energy stability for phase-field models, since the locally Lipschitz continuous nonlinear term usually becomes fully Lipschitz continuous thanks to the uniform pointwise bound. For instance, the Allen–Cahn equation can be viewed as the L^2 gradient flow associating with the energy

$$E(u) = \int \left(\frac{\varepsilon^2}{2} |\nabla u(\boldsymbol{x})|^2 + \frac{1}{4}(u^2(\boldsymbol{x}) - 1)^2 \right) \mathrm{d}\boldsymbol{x}, \tag{2}$$

and the solution satisfies the energy stability in the sense that the energy is non-increasing in time, namely, $E(u(t_2)) \leq E(u(t_1))$ for any $t_2 \geq t_1 \geq 0$. There have been a large variety of numerical schemes preserving such energy stability successfully applied on different types of phase-field models, e.g., [9,17,21,27,33,35–37,45,47,49] and the references therein. It was found that the MBP plays a key role to show such nonlinear energy stability [10,24,34,42].

Recently, MBP-preserving numerical schemes have attracted increasingly attentions for semilinear parabolic equations in the form of (1). In [40], it was shown for the Allen–Cahn equation in one-dimensional case that the MBP was preserved by the central difference semi-discrete scheme and its fully discrete approximations with forward and backward Euler time-stepping methods. Later, the discrete MBPs, as well as the energy stability, of the first- and second-order stabilized semi-implicit (SSI) schemes with central difference method were proved for the Allen–Cahn equation in [23,34,42], and those of the SSI schemes with finite element discretization in space were obtained for the surface Allen–Cahn equation in [46]. The discrete MBPs were also obtained for the Allen–Cahn equation in [15] by first-order exponential time differencing (ETD) scheme in space-continuous setting, in [25] by second-order nonlinear implicit-explicit schemes with spatial central difference method, and in [48] by showing the uniform L^p boundedness and passing the limit as p goes to infinity. In addition, MBP-preserving numerical schemes have been studied for the nonlocal Allen–Cahn equation by using first- and second-order ETD schemes [10] combined with a quadrature-based difference method [13], for the space-fractional Allen–Cahn equation by using the Crank–Nicolson scheme [24] with central difference approximation [44], for the time-fractional Allen–Cahn equation by using the convex splitting methods [14], and for the complex-valued Ginzburg–Landau model of superconductivity [8] by considering the finite volume method [5,18] and finite element method with the mass-lumping technique [6] in space with backward Euler time integration. In [43], Tang and Yang proposed so-called one-step monotone schemes to check whether or not a scheme is MBP-preserving, in which the regular third-order explicit strong stability-preserving (SSP) method [20] is shown to be MBP-preserving for the Allen–Cahn equation with a CFL condition as $\tau = \mathcal{O}(h^2)$. An abstract framework on the MBP for equations like (1) was established in the recent work [11], where sufficient conditions for linear and nonlinear operators were given such that the equation satisfies the MBP and the corresponding first- and second-order ETD schemes preserve the MBP. Some details on the framework will be given in Section 2.

In this paper, we investigate high-order MBP-preserving time integration schemes. The integrating factor Runge–Kutta (IFRK) method is used for the time integration, which has been widely studied for stiff ordinary differential equations (ODEs) recently [1,28,41]. The IFRK method can be viewed as an extension of the conventional Runge–Kutta (RK) method, particularly designed for the case that the problem contains linear part with strong stiffness. The key idea is to use the exponential integrating factor to eliminate the stiff linear term and apply the conventional RK method to the resulted system. To study the stability of the IFRK method, the concept of strong stability-preserving (SSP) was proposed in [38] to construct efficient time discretization for hyperbolic conservation laws and then further explored in [19] for high-order schemes. The SSP property means that the norm of the numerical solution diminishes. More precisely, for an ODE system taking the form

$$\frac{\mathrm{d}u}{\mathrm{d}t} = Lu + N(u) \tag{3}$$

with the matrix L and the mapping N satisfying

$$\|e^{\omega L}\| \le 1, \quad \forall\, \omega > 0 \tag{4}$$

and, for some $\omega_0 > 0$,

$$\|u + \omega N(u)\| \le \|u\|, \quad \forall\, \omega \in (0, \omega_0], \tag{5}$$

the IFRK method for (3) is called SSP if its solution satisfies $\|u^{n+1}\| \le \|u^n\|$. A review of the SSP-RK time discretization method was presented in [20] for ODE systems like (3) with $L = 0$, which were often derived from spatial discretization of hyperbolic conservation law equations, and a recent work [26] generalized these results to the general case of the SSP-IFRK method for (3). The general form of the SSP-RK method for (3) with $L = 0$ is given by

$$\begin{aligned} &u^{(i)} = \sum_{j=0}^{i-1} \left[\alpha_{ij} u^{(j)} + \tau \beta_{ij} N(u^{(j)}) \right], \quad 1 \le i \le s, \\ &\text{with } u^{(0)} = u^n, \ u^{n+1} = u^{(s)}, \end{aligned} \tag{6}$$

where α_{ij} are nonnegative. Here, (6) is actually a convex combination of some forward Euler sub-steps with the step sizes $\tau \frac{\beta_{ij}}{\alpha_{ij}}$ and the nonnegativity of β_{ij} is crucial to guarantee (5). It is concluded in [19,20] that, under the constraint of the nonnegativity of β_{ij}, there is no SSP-RK method with order higher than four and the number of stage for fourth-order SSP-RK methods cannot be lower than five.

The main contribution of this work includes three aspects. First, we formulate the general results for the IFRK method preserving the MBP for equations like (1) under the abstract framework established in the recent work [11]. For simplicity, we restrict our discussion on the space-discrete version to avoid the abstract and tedious definitions of continuous function spaces and domains of operators. Second, we give the error estimates of the numerical solution to the MBP-preserving IFRK method by utilizing the uniform L^∞ boundedness guaranteed by the MBP. Third, we identify some three-stage, third-order and four-stage, fourth-order MBP-preserving IFRK schemes. To the best of our knowledge, this is the first time to present a fourth-order numerical scheme being able to preserve the MBP, and this fills the gap of the lack of MBP-preserving numerical schemes with order higher than three. The requirements on the time step size for preserving the MBP have the same magnitudes as the first-order IF scheme, and are contributed only from the nonlinear term without the CFL restriction. Numerical experiments also show the high efficiency of the four-stage, fourth-order IFRK scheme.

The rest of this paper is organized as follows. In Section 2, we briefly restate the sufficient conditions determined in [11] for the linear and nonlinear operators such that equation (1) satisfies the MBP. We also give the space-discrete equation of (1) and the corresponding conditions of the linear and nonlinear parts in the discrete setting. Then, in Section 3, we present the IFRK method in the general form and prove the preservation of the MBP and the error estimates of the method under some certain requirement on the time step size. In particular, we present a four-stage, fourth-order IFRK scheme which is MBP preserving and give some simple examples of the space-discrete system. In Section 4, some numerical experiments are carried out for the reaction-diffusion equation with a logarithmic nonlinear term or a monotonic source term, including the tests of convergence rate, MBP, and efficiency for 2D and 3D long-time simulations. Finally, some concluding remarks are given in Section 5.

2. Maximum bound principle for semilinear parabolic equations

An abstract framework on the maximum bound principle for a class of semilinear parabolic equations (1) was established in [11], where sufficient conditions for the linear and nonlinear operators were given such that equation (1) satisfies the MBP. For the completeness of the current paper, we present some main results in [11]. Denote by Ω the spatial domain as usual.

A crucial condition on the linear operator $\mathcal{L}$ is the dissipativity in the sense that if a function w reaches its maximum on $\overline{\Omega}$ at a point $\boldsymbol{x}_0 \in \Omega$, then it must hold $\mathcal{L}w(\boldsymbol{x}_0) \le 0$. By defining the function space X appropriately, this condition implies that $\mathcal{L}$ is the generator of a contraction semigroup on X. Such $\mathcal{L}$ can be the standard Laplace operator, nonlocal diffusion operator [7], fractional Laplace operator [29] and so on. The nonlinear operator $\mathcal{N}$ is assumed to act as a composite function, i.e., $\mathcal{N}[w](\boldsymbol{x}) = f(w(\boldsymbol{x}))$ for any function w and $\boldsymbol{x} \in \overline{\Omega}$, where f is a given one-variable continuously differentiable function satisfying

$$f(\rho) \le 0 \le f(-\rho), \quad \text{for some constant } \rho > 0. \tag{7}$$

The essential point is the change of the sign of f on both sides of zero. Under these assumptions, equation (1) satisfies the MBP, that is, if the absolute values of initial and boundary conditions are bounded by ρ, then the absolute value of the solution is also pointwise bounded by ρ for all time.

Applying some type of spatial discretization to (1), one can obtain the space-discrete problem given by the ordinary differential equation (ODE) system

$$\frac{du}{dt} = Lu + f(u). \tag{8}$$

Here, $u(t) = (u_1(t), u_2(t), \ldots, u_m(t))^T \in \mathbb{R}^m$ denotes the space-discrete solution, L is an m-by-m symmetric matrix derived from the spatial discretization of the linear operator $\mathcal{L}$, and the vector $f(u)$ with the j-th component $f(u_j)$ corresponds to the nonlinear term $\mathcal{N}[u]$. We denote by $\|\cdot\|_\infty$ the vector or matrix ∞-norm as usual. The framework developed in [11] also consists of the space-discrete problem (8). Therefore, we require that the matrix L is the generator of a contraction semigroup on $\mathbb{R}^m$, or equivalently,

$$\|e^{\omega L}\|_\infty \le 1, \quad \forall\, \omega > 0, \tag{9}$$

which is identical to (4). For the nonlinear function f, due to the assumption (7), i.e., the change of the sign of f on both sides of zero, the following condition holds:

$$\exists\, \omega_0^+ > 0 \text{ such that } |\xi + \omega f(\xi)| \le \rho, \forall\, \xi \in [-\rho, \rho], \forall\, \omega \in (0, \omega_0^+], \tag{10}$$

which is weaker than (5). Sometimes, we also need to further assume:

$$\exists\, \omega_0^- > 0 \text{ such that } |\xi - \omega f(\xi)| \le \rho, \forall\, \xi \in [-\rho, \rho], \forall\, \omega \in (0, \omega_0^-]. \tag{11}$$

Remark 2.1. The condition (11) is very crucial to remove the nonnegativity requirement of the coefficients β_{ij} as we mentioned in the standard SSP-RK schemes (6). This allows us to show that the four-stage, fourth-order IFRK scheme is actually MBP-preserving for the model equation (8) satisfying (7), which will be demonstrated in the following section.

3. Integrating factor Runge–Kutta method

In this section, we will present a family of IFRK schemes for time-stepping of the space-discrete system (8). The method is based on the Runge–Kutta time discretizations combined with the exponential integrating factor. We will show the MBP-preserving property under the conditions (9)–(11) and the error estimates of the numerical solutions.

3.1. MBP-preserving IFRK method in general form

We have claimed that L in (8) is an m-by-m matrix corresponding to the spatial discretization of the linear operator $\mathcal{L}$. Premultiplying the system (8) by e^{-tL}, we have

$$\frac{d(e^{-tL}u)}{dt} = e^{-tL} f(u).$$

Defining a transformation of variables by $w = e^{-tL}u$, we obtain a new ODE system

$$\frac{dw}{dt} = e^{-tL} f(e^{tL} w) =: G(t, w). \tag{12}$$

The general explicit s-stage Runge–Kutta method for (12) is given by [38]

$$w^{(0)} = w^n, \tag{13a}$$

$$w^{(i)} = w^{(0)} + \tau \sum_{j=0}^{i-1} d_{ij} G(t_n + c_j \tau, w^{(j)}), \quad 1 \le i \le s, \tag{13b}$$

$$w^{n+1} = w^{(s)}, \tag{13c}$$

where $c_0 = 0$, $c_i = \sum_{j=0}^{i-1} d_{ij}$ for $1 \le i \le s$, and $c_s = 1$ for consistency. For $\alpha_{ij} \ge 0$ to be determined such that $\sum_{j=0}^{i-1} \alpha_{ij} = 1$, we rewrite (13b) as

$$w^{(i)} = \sum_{j=0}^{i-1} [\alpha_{ij} w^{(j)} + \tau \beta_{ij} G(t_n^{(j)}, w^{(j)})], \quad 1 \le i \le s, \tag{14}$$

where $\beta_{ij} = d_{ij} - \sum_{k=j+1}^{i-1} \alpha_{ik} d_{kj}$ and $t_n^{(j)} = t_n + c_j \tau$. If we require that $\beta_{ij} = 0$ when its corresponding $\alpha_{ij} = 0$, then (14) is a convex combination of a group of forward Euler substeps

$$w^{(j)} + \tau \frac{\beta_{ij}}{\alpha_{ij}} G(t_n^{(j)}, w^{(j)}).$$

Define $u^n = e^{t_n L} w^n$ and $u^{(i)} = e^{t_n^{(i)} L} w^{(i)}$, $0 \le i \le s$, then (14) becomes

$$u^{(i)} = \sum_{j=0}^{i-1} e^{(c_i - c_j)\tau L} [\alpha_{ij} u^{(j)} + \tau \beta_{ij} f(u^{(j)})], \quad 1 \le i \le s,$$

which can be viewed as a convex combination of the exponential forward Euler substeps

$$e^{(c_i - c_j)\tau L} \Big[u^{(j)} + \tau \frac{\beta_{ij}}{\alpha_{ij}} f(u^{(j)}) \Big].$$

Now, we obtain the following s-stage IFRK method for (8):

$$u^{(0)} = u^n, \tag{15a}$$

$$u^{(i)} = \sum_{j=0}^{i-1} e^{(c_i - c_j)\tau L} [\alpha_{ij} u^{(j)} + \tau \beta_{ij} f(u^{(j)})], \quad 1 \le i \le s, \tag{15b}$$

$$u^{n+1} = u^{(s)}. \tag{15c}$$

The main result on the MBP-preserving property of (15) is as follows.

Theorem 3.1. *Given a linear operator L satisfying (9), a function f satisfying (10) and (11), and the abscissas $\{c_j\}$ satisfying*

$$c_0 \le c_1 \le \cdots \le c_s, \tag{16}$$

if $\|u^n\|_\infty \le \rho$, then u^{n+1} obtained from (15) satisfies $\|u^{n+1}\|_\infty \le \rho$, provided that the time step size satisfies

$$\tau \le \mathcal{C} \omega_0^+, \quad \text{with } \mathcal{C} = \min_{i,j} \frac{\alpha_{ij}}{\beta_{ij}} \tag{17}$$

when β_{ij} are all nonnegative, or satisfies

$$\tau \le \mathcal{C} \min\{\omega_0^+, \omega_0^-\}, \quad \text{with } \mathcal{C} = \min_{i,j} \frac{\alpha_{ij}}{|\beta_{ij}|} \tag{18}$$

whenever there is a negative β_{ij}.

Proof. For each stage of (15), suppose $\|u^{(j)}\|_\infty \le \rho$ for all $j \le i-1$. Then, we have

$$\begin{aligned}
\|u^{(i)}\|_\infty &\le \sum_{j=0}^{i-1} \|e^{(c_i - c_j)\tau L} [\alpha_{ij} u^{(j)} + \tau \beta_{ij} f(u^{(j)})]\|_\infty \\
&\le \sum_{j=0}^{i-1} \alpha_{ij} \|e^{(c_i - c_j)\tau L}\|_\infty \Big\| u^{(j)} + \tau \frac{\beta_{ij}}{\alpha_{ij}} f(u^{(j)}) \Big\|_\infty \\
&\le \sum_{j=0}^{i-1} \alpha_{ij} \cdot \rho \\
&= \rho,
\end{aligned}$$

since $c_i - c_j \ge 0$, and $\tau \max_{i,j} \frac{\beta_{ij}}{\alpha_{ij}} \le \omega_0^+$ or $\tau \max_{i,j} \frac{|\beta_{ij}|}{\alpha_{ij}} \le \min\{\omega_0^+, \omega_0^-\}$. By induction, we obtain $\|u^{(i)}\|_\infty \le \rho$ for each i, and thus $\|u^{n+1}\| \le \rho$. □

Remark 3.1. Condition (16) implies the property of *non-decreasing abscissas*, which is crucial for the preservation of the MBP for the IFRK method (15).

3.2. Error estimate

To carry out convergence analysis for the IFRK method (15), we transform the variable w in (13) back to u to get

$$u^{(0)} = u^n, \tag{19a}$$

$$u^{(i)} = \mathrm{e}^{c_i\tau L}u^n + \tau\sum_{j=0}^{i-1} d_{ij}\mathrm{e}^{(c_i-c_j)\tau L}f(u^{(j)}), \quad 1 \le i \le s-1, \tag{19b}$$

$$u^{n+1} = \mathrm{e}^{\tau L}u^n + \tau\sum_{i=0}^{s-1} d_{si}\mathrm{e}^{(1-c_i)\tau L}f(u^{(i)}). \tag{19c}$$

For simplicity, we do not introduce the general order conditions for arbitrary-order RK methods (see, e.g., [22]). Instead, we suppose directly that the RK method (13) is p-th order, where $1 \le p \le s$. Then, we have the following error estimate for (19).

Theorem 3.2. *Given $T > 0$, suppose that the exact solution, denoted by $u_e(t)$, of (8) is sufficiently smooth on $[0, T]$ and f is p-times continuously differentiable on $[-\rho, \rho]$. Under the conditions of Theorem 3.1, if the time step size τ satisfies (17) and (18), then the numerical solution u^n generated by the IFRK method (19) with $u^0 = u_e(0)$ and $\|u_e(0)\|_\infty \le \rho$ satisfies the error estimate:*

$$\|u_e(t_n) - u^n\|_\infty \le C(\mathrm{e}^{F_1 s t_n} - 1)\tau^p, \quad t_n \le T,$$

where $F_1 = \max\limits_{|\xi|\le\rho} |f'(\xi)|$ and the constant $C > 0$ is independent of τ.

Proof. Following [12,50], let us introduce the reference functions $v^{(i)}$ satisfying

$$v^{(0)} = u_e(t_n), \tag{20a}$$

$$v^{(i)} = \mathrm{e}^{c_i\tau L}u_e(t_n) + \tau\sum_{j=0}^{i-1} d_{ij}\mathrm{e}^{(c_i-c_j)\tau L}f(v^{(j)}), \quad 1 \le i \le s-1, \tag{20b}$$

$$u_e(t_{n+1}) = \mathrm{e}^{\tau L}u_e(t_n) + \tau\sum_{i=0}^{s-1} d_{si}\mathrm{e}^{(1-c_i)\tau L}f(v^{(i)}) + \tau R^n, \tag{20c}$$

where the truncation error R^n satisfies

$$\max_{0\le n\le[T/\tau]} \|R^n\|_\infty \le \widetilde{C}\tau^p, \tag{21}$$

where the constant $\widetilde{C} > 0$ depends on the $C^{p+1}[0, T]$-norm of u_e, the $C^p[-\rho, \rho]$-norm of f, $\|L\|_\infty$, T, p, and s, but is independent of τ. Note that $\|u_e(t)\|_\infty \le \rho$ for any $t \in [0, T]$ due to the MBP of (8). According to (20a) and (20b), we know from the proof of Theorem 3.1 that $\|v^{(i)}\|_\infty \le \rho$ for each $i = 1, 2, \ldots, s-1$. Let $e^n = u_e(t_n) - u^n$ and $e^{(i)} = v^{(i)} - u^{(i)}$ for $i = 0, 1, \ldots, s-1$.

For each $i = 1, 2, \ldots, s-1$, the difference between (20b) and (19b) gives

$$e^{(i)} = \mathrm{e}^{c_i\tau L}e^n + \tau\sum_{j=0}^{i-1} d_{ij}\mathrm{e}^{(c_i-c_j)\tau L}[f(v^{(j)}) - f(u^{(j)})].$$

Using (9) and noting $d_{ij} \le c_i \le 1$, we obtain

$$\|e^{(i)}\|_\infty \le \|e^n\|_\infty + \tau\sum_{j=0}^{i-1}\|f(v^{(j)}) - f(u^{(j)})\|_\infty \le \|e^n\|_\infty + F_1\tau\sum_{j=0}^{i-1}\|e^{(j)}\|_\infty.$$

By induction, assuming $\|e^{(j)}\|_\infty \le (1 + F_1\tau)^j\|e^n\|_\infty$ for $j = 0, 1, \ldots, i-1$, we obtain

$$\|e^{(i)}\|_\infty \le \|e^n\|_\infty + F_1\tau\sum_{j=0}^{i-1}(1 + F_1\tau)^j\|e^n\|_\infty = (1 + F_1\tau)^i\|e^n\|_\infty. \tag{22}$$

Therefore, the inequality (22) holds for any $i = 0, 1, 2, \ldots, s-1$.

Similarly, the difference between (20c) and (19c) leads to

$$e^{n+1} = \mathrm{e}^{\tau L} e^n + \tau \sum_{i=0}^{s-1} d_{si} \mathrm{e}^{(1-c_i)\tau L}[f(v^{(i)}) - f(u^{(i)})] + \tau R^n,$$

and then, using (22) and (21), it yields

$$\begin{aligned}
\|e^{n+1}\|_\infty &\le \|e^n\|_\infty + F_1 \tau \sum_{i=0}^{s-1} \|e^{(i)}\|_\infty + \tau \|R^n\|_\infty \\
&\le \|e^n\|_\infty + F_1 \tau \sum_{i=0}^{s-1} (1 + F_1\tau)^i \|e^n\|_\infty + \widetilde{C}\tau^{p+1} \\
&= (1 + F_1\tau)^s \|e^n\|_\infty + \widetilde{C}\tau^{p+1}.
\end{aligned}$$

By recursion, we obtain

$$\|e^n\|_\infty \le (1 + F_1\tau)^{ns} \|e^0\|_\infty + \widetilde{C}\tau^{p+1} \sum_{k=0}^{n-1} (1 + F_1\tau)^{ks}.$$

Noting that $e^0 = 0$ and denoting $C = \widetilde{C}(F_1 s)^{-1}$, we have

$$\|e^n\|_\infty \le C\tau^p[(1 + F_1\tau)^{ns} - 1] \le C(\mathrm{e}^{F_1 s t_n} - 1)\tau^p,$$

which completes the proof. □

In addition to the MBP property, a special L^∞ stability, there is another type of stability for the semilinear parabolic equation

$$u_t = \mathcal{L}u + f(u), \tag{23}$$

a special case of (1), where $\mathcal{L}$ is a dissipative operator and f is a one-variable function as we assumed in Section 2. By defining a functional E as

$$E(u) = -\frac{1}{2}(u, \mathcal{L}u)_{L^2} + \int_\Omega F(u(\boldsymbol{x}))\, \mathrm{d}\boldsymbol{x},$$

where F is a one-variable function satisfying $F' = -f$, one can verify that (23) is exactly the L^2 gradient flow with respect to E, and thus, the solution to (23) satisfies

$$\frac{\mathrm{d}}{\mathrm{d}t} E(u(t)) \le 0, \quad t > 0.$$

This property is usually called energy stability or energy dissipation, and E is called the energy functional corresponding to (23). For the space-discrete problem (8), the energy stability is still valid with respect to the space-discrete energy functional denoted by E_h. There are some difficulties in proving the discrete energy dissipation of the IFRK schemes (15), but we can give the uniform bound of the discrete energy by applying the result of the error estimates. By carrying out the similar analysis as [10,11], when τ is small enough, we can obtain

$$E_h(u^n) \le E_h(u^0) + C, \quad \forall n,$$

where the constant $C > 0$ is independent of τ. Nevertheless, the discrete energy dissipation can still be observed in the numerical simulations shown in Section 4.

3.3. Various MBP-preserving IFRK schemes

We have shown the MBP-preserving property for the IFRK method in the general form. Now, we present some concrete and practical MBP-preserving IFRK schemes under the general results established above. We use the vector $c = [c_0, c_1, \ldots, c_s]^T$ to denote the sequence of abscissas.

Scheme 1 *(IF1). The first-order integrating factor (IF1) scheme for solving* (8) *reads [26]*

$$u^{n+1} = \mathrm{e}^{\tau L}[u^n + \tau f(u^n)]. \tag{24}$$

Here, $c = [0, 1]^T$, $\beta_{ij} > 0$, *and* $\mathcal{C} = 1$. *Thus, the condition* (17) *becomes*

$$\tau \le \omega_0^+. \tag{25}$$

Scheme 2 *(IFRK2). A second-order integrating factor Runge–Kutta (IFRK2) scheme for solving* (8) *reads [26]*

$$\begin{aligned} u^{(1)} &= \mathrm{e}^{\tau L}[u^n + \tau f(u^n)] \\ &= \mathrm{e}^{\tau L}u^n + \tau \mathrm{e}^{\tau L} f(u^n), \end{aligned} \tag{26a}$$

$$\begin{aligned} u^{n+1} &= \frac{1}{2}\mathrm{e}^{\tau L}u^n + \frac{1}{2}[u^{(1)} + \tau f(u^{(1)})] \\ &= \mathrm{e}^{\tau L}u^n + \tau\Big(\frac{1}{2}\mathrm{e}^{\tau L} f(u^n) + \frac{1}{2} f(u^{(1)})\Big). \end{aligned} \tag{26b}$$

Here, $c = [0, 1, 1]^T$, $\beta_{ij} \ge 0$, *and* $\mathcal{C} = 1$. *Thus, the condition* (17) *is the same as* (25).

Scheme 3 *(IFRK3). A third-order integrating factor Runge–Kutta (IFRK3) scheme for solving* (8) *reads [26]*

$$\begin{aligned} u^{(1)} &= \frac{1}{2}\mathrm{e}^{\frac{2\tau}{3}L}u^n + \frac{1}{2}\mathrm{e}^{\frac{2\tau}{3}L}\Big[u^n + \frac{4\tau}{3} f(u^n)\Big] \\ &= \mathrm{e}^{\frac{2\tau}{3}L}u^n + \frac{2\tau}{3}\mathrm{e}^{\frac{2\tau}{3}L} f(u^n), \end{aligned} \tag{27a}$$

$$\begin{aligned} u^{(2)} &= \frac{2}{3}\mathrm{e}^{\frac{2\tau}{3}L}u^n + \frac{1}{3}\Big[u^{(1)} + \frac{4\tau}{3} f(u^{(1)})\Big] \\ &= \mathrm{e}^{\frac{2\tau}{3}L}u^n + \frac{2\tau}{3}\Big(\frac{1}{3}\mathrm{e}^{\frac{2\tau}{3}L} f(u^n) + \frac{2}{3} f(u^{(1)})\Big), \end{aligned} \tag{27b}$$

$$\begin{aligned} u^{n+1} &= \frac{59}{128}\mathrm{e}^{\tau L}u^n + \frac{15}{128}\mathrm{e}^{\tau L}\Big[u^n + \frac{4\tau}{3} f(u^n)\Big] + \frac{27}{64}\mathrm{e}^{\frac{\tau}{3}L}\Big[u^{(2)} + \frac{4\tau}{3} f(u^{(2)})\Big] \\ &= \mathrm{e}^{\tau L}u^n + \tau\Big(\frac{4}{16}\mathrm{e}^{\tau L} f(u^n) + \frac{3}{16}\mathrm{e}^{\frac{\tau}{3}L} f(u^{(1)}) + \frac{9}{16}\mathrm{e}^{\frac{\tau}{3}L} f(u^{(2)})\Big). \end{aligned} \tag{27c}$$

Here, $c = [0, \frac{2}{3}, \frac{2}{3}, 1]^T$, $\beta_{ij} \ge 0$, *and* $\mathcal{C} = \frac{3}{4}$. *Thus, the condition* (17) *leads to*

$$\tau \le \frac{3}{4}\omega_0^+. \tag{28}$$

Remark 3.2. Applying the third-order Shu–Osher method [38] to (12) gives

$$\begin{aligned} u^{(1)} &= \mathrm{e}^{\tau L}[u^n + \tau f(u^n)] \\ &= \mathrm{e}^{\tau L}u^n + \tau \mathrm{e}^{\tau L} f(u^n), \end{aligned} \tag{29a}$$

$$\begin{aligned} u^{(2)} &= \frac{3}{4}\mathrm{e}^{\frac{\tau}{2}L}u^n + \frac{1}{4}\mathrm{e}^{-\frac{\tau}{2}L}[u^{(1)} + \tau f(u^{(1)})] \\ &= \mathrm{e}^{\frac{\tau}{2}L}u^n + \frac{\tau}{2}\Big(\frac{1}{2}\mathrm{e}^{\frac{\tau}{2}L} f(u^n) + \frac{1}{2}\mathrm{e}^{-\frac{\tau}{2}L} f(u^{(1)})\Big), \end{aligned} \tag{29b}$$

$$\begin{aligned} u^{n+1} &= \frac{1}{3}\mathrm{e}^{\tau L}u^n + \frac{2}{3}\mathrm{e}^{\frac{\tau}{2}L}[u^{(2)} + \tau f(u^{(2)})] \\ &= \mathrm{e}^{\tau L}u^n + \tau\Big(\frac{1}{6}\mathrm{e}^{\tau L} f(u^n) + \frac{2}{3}\mathrm{e}^{\frac{\tau}{2}L} f(u^{(2)}) + \frac{1}{6} f(u^{(1)})\Big), \end{aligned} \tag{29c}$$

which gives $c = [0, 1, \frac{1}{2}, 1]^T$, $\beta_{ij} \ge 0$, and $\mathcal{C} = 1$. There is a matrix exponential with a negative coefficient due to the existence of decreasing abscissas, so this scheme may not preserve the MBP. We will show in Section 4 that the scheme (29) does not preserve the MBP even though a small time step size is used. This suggests the necessity of the property of non-decreasing abscissas.

Apart from the three-stage IFRK3 scheme (27), one can give more MBP-preserving third-order IFRK schemes by combining the exponential integrating factor approach with the RK method with non-decreasing abscissas, e.g., eSSPRK$^+$(4,3) in [26].

Scheme 4 *(IFRK4). Applying the classic fourth-order Runge–Kutta method to* (12) *gives the fourth-order integrating factor Runge–Kutta (IFRK4) scheme:*

$$\begin{aligned} u^{(1)} &= \mathrm{e}^{\frac{\tau}{2}L}\Big[u^n + \frac{\tau}{2} f(u^n)\Big] \\ &= \mathrm{e}^{\frac{\tau}{2}L} u^n + \frac{\tau}{2}\mathrm{e}^{\frac{\tau}{2}L} f(u^n), \end{aligned} \tag{30a}$$

$$\begin{aligned} u^{(2)} &= \frac{1}{2}\mathrm{e}^{\frac{\tau}{2}L}\Big[u^n - \frac{\tau}{2} f(u^n)\Big] + \frac{1}{2}[u^{(1)} + \tau f(u^{(1)})] \\ &= \mathrm{e}^{\frac{\tau}{2}L} u^n + \frac{\tau}{2} f(u^{(1)}), \end{aligned} \tag{30b}$$

$$\begin{aligned} u^{(3)} &= \frac{1}{9}\mathrm{e}^{\tau L}[u^n - \tau f(u^n)] + \frac{2}{9}\mathrm{e}^{\frac{\tau}{2}L}\Big[u^{(1)} - \frac{3\tau}{2} f(u^{(1)})\Big] + \frac{2}{3}\mathrm{e}^{\frac{\tau}{2}L}\Big[u^{(2)} + \frac{3\tau}{2} f(u^{(2)})\Big] \\ &= \mathrm{e}^{\tau L} u^n + \tau \mathrm{e}^{\frac{\tau}{2}L} f(u^{(2)}), \end{aligned} \tag{30c}$$

$$\begin{aligned} u^{n+1} &= \frac{1}{3}\mathrm{e}^{\frac{\tau}{2}L}\Big[u^{(1)} + \frac{\tau}{2} f(u^{(1)})\Big] + \frac{1}{3}\mathrm{e}^{\frac{\tau}{2}L} u^{(2)} + \frac{1}{3}\Big[u^{(3)} + \frac{\tau}{2} f(u^{(3)})\Big] \\ &= \mathrm{e}^{\tau L} u^n + \tau\Big(\frac{1}{6}\mathrm{e}^{\tau L} f(u^n) + \frac{1}{3}\mathrm{e}^{\frac{\tau}{2}L} f(u^{(1)}) + \frac{1}{3}\mathrm{e}^{\frac{\tau}{2}L} f(u^{(2)}) + \frac{1}{6} f(u^{(3)})\Big). \end{aligned} \tag{30d}$$

Here, $c = [0, \frac{1}{2}, \frac{1}{2}, 1, 1]^T$, $\mathcal{C} = \frac{2}{3}$, *and* β_{ij} *are not all nonnegative. Thus, the condition* (18) *yields*

$$\tau \le \frac{2}{3}\min\{\omega_0^+, \omega_0^-\}. \tag{31}$$

As illustrated in [19], the constraint of the nonnegativity of β_{ij} leads to the nonexistence of four-stage, fourth-order SSP-IFRK schemes. In our work, however, the conditions (10) and (11) relax the requirement of the nonnegative β_{ij}. Therefore, the IFRK4 scheme (30) is adequate to preserve the MBP without any needs of extra computations for the modification of f as done in [38]. More MBP-preserving fourth-order IFRK schemes with larger numbers of stage can be obtained by using, for example, eSSPRK$^+$(5,4) and eSSPRK$^+$(10,4) presented in [26].

Since ω_0^+ and ω_0^- are completely determined by f via (10) and (11), from the inequalities (25), (28), and (31), we find that the constraints on the time step sizes depend only on f but not on the size of L. This means that the choice of the time step sizes is independent of the spatial mesh size. Moreover, we point out that these constraints are all sufficient but not necessary conditions for the MBP-preserving property.

3.4. Examples of the matrix L and the function f

A large number of examples of linear and nonlinear operators in (1) have been shown to satisfy the assumptions made in [11], including the space-continuous and space-discrete cases, and thus, we can check the matrix L in (8) in the same way. Here, we present a more direct criterion for L from the point of view of matrices.

Lemma 3.3 *([3,39]). For any matrix* $A = (a_{ij}) \in \mathbb{R}^{m\times m}$ *and any constant* $s \ge 0$, *we have*

$$\|\mathrm{e}^{sA}\|_\infty \le \mathrm{e}^{s\mu_\infty(A)},$$

where $\mu_\infty(A)$ *is the logarithmic norm of* A *with respect to the* ∞*-norm, i.e.,*

$$\mu_\infty(A) = \max_{1\le i\le m}\left(a_{ii} + \sum_{\substack{j=1\\ j\ne i}}^{m} |a_{ij}|\right).$$

Remark 3.3. If A is diagonally dominant with all diagonal entries negative, then we have $\|\mathrm{e}^{sA}\|_\infty \le 1$ for any $s \ge 0$ since $\mu_\infty(A) \le 0$. See the following example.

Example 3.1. If L is given by the one-dimensional second-order central difference discretization of Δ, i.e.,

$$L = \frac{1}{h^2}\begin{pmatrix} -2 & 1 & & & c \\ 1 & -2 & 1 & & \\ & \ddots & \ddots & \ddots & \\ & & 1 & -2 & 1 \\ c & & & 1 & -2 \end{pmatrix} \quad \text{with } c = 0 \text{ or } c = 1,$$

then $\mu_\infty(L) = 0$ and $\mu_\infty(-L) = 4/h^2$. According to Lemma 3.3, we have

$$\|e^{\tau L}\|_\infty \le 1, \qquad \|e^{-\tau L}\|_\infty \le e^{\frac{4\tau}{h^2}}.$$

Denoting by I the identity matrix with the same size as L and in the two-dimensional case letting

$$L^{(2)} = I \otimes L + L \otimes I, \tag{32}$$

we have $\mu_\infty(L^{(2)}) = 0$ and $\mu_\infty(-L^{(2)}) = 8/h^2$, and thus,

$$\|e^{\tau L^{(2)}}\|_\infty \le 1, \qquad \|e^{-\tau L^{(2)}}\|_\infty \le e^{\frac{8\tau}{h^2}}. \tag{33}$$

The three-dimensional case

$$L^{(3)} = I \otimes I \otimes L + I \otimes L \otimes I + L \otimes I \otimes I \tag{34}$$

is quite similar.

To guarantee (10) and (11) for the nonlinear function f, we actually have the following result. The proof is straightforward, so we omit it.

Proposition 3.4. *If there exists $\rho > 0$ such that $f(\pm\rho) = 0$ and f is continuously differentiable and nonconstant on $[-\rho, \rho]$, then (10) and (11) hold respectively for*

$$\omega_0^+ = -\frac{1}{\min\limits_{|\xi|\le\rho} f'(\xi)} \quad \text{and} \quad \omega_0^- = \frac{1}{\max\limits_{|\xi|\le\rho} f'(\xi)}.$$

Example 3.2. The Allen–Cahn equation has the nonlinear term $f(u) = u - u^3$, which satisfies (10) and (11) with $\rho = 1, \omega_0^+ = \frac{1}{2}$, and $\omega_0^- = 1$.

Example 3.3. Given the Flory–Huggins potential function

$$F(u) = \frac{\theta}{2}[(1+u)\ln(1+u) + (1-u)\ln(1-u)] - \frac{\theta_c}{2}u^2, \tag{35}$$

where θ and θ_c are two positive constants satisfying $\theta < \theta_c$. We set $f(u) = -F'(u)$, namely,

$$f(u) = \frac{\theta}{2}\ln\frac{1-u}{1+u} + \theta_c u. \tag{36}$$

Denote by γ the positive root of $f(\gamma) = 0$. Noting that

$$\max_{|\xi|\le\gamma} f'(\xi) = \theta_c - \theta > 0, \qquad \min_{|\xi|\le\gamma} f'(\xi) = \theta_c - \frac{\theta}{1-\gamma^2} < 0,$$

we know f satisfies (10) and (11) with $\rho = \gamma$, $\omega_0^+ = \frac{1-\gamma^2}{\theta - \theta_c(1-\gamma^2)}$, and $\omega_0^- = \frac{1}{\theta_c - \theta}$.

Example 3.4. Consider $f(u) = a - e^u$, where $a > 0$ is a constant. Different from two examples given above, $f(u)$ is strictly monotonic in u with $\ln a$ the unique zero point. We can choose $\rho \ge |\ln a|$ if $a \ne 1$, or any $\rho > 0$ if $a = 1$, to satisfy (7). For either case, some detailed calculations suggest that

$$\omega_0^+ = \min\left\{\frac{1}{a}, \frac{2\rho}{e^\rho - a}\right\} \tag{37}$$

satisfies (10). However, there is no $\omega_0^- > 0$ such that (11) holds, which means that the IFRK4 scheme (30) cannot be applied to this case since it contains some negative β_{ij}.

The model (1) with $f(u) = a - e^u$ is not a typical gradient flow as the well-known Allen–Cahn equation, and it is easy to verify that the steady state solution is the constant function $u \equiv \ln a$. When $a \neq 1$, equation (1) with $f(u) = a - e^u$ satisfies the MBP with the bounding constant $\rho \geq |\ln a|$. When $a = 1$, a stronger stability is satisfied, i.e., the absolute value of the solution must reach its maximum at the initial time or on the boundary, which is obvious if we set ρ to be the maximum of the absolute value of the initial and boundary values. In particular, if we enforce the periodic, homogeneous Dirichlet, or homogeneous Neumann boundary condition, then the supremum norm of the solution is monotonically nonincreasing in time.

4. Numerical experiments

Let us consider the reaction-diffusion equation

$$u_t = \varepsilon^2 \Delta u + f(u), \quad (x, y) \in \Omega = (0, 1)^d, \ t \in (0, T], \tag{38}$$

with $d = 2$ or 3, subject to the periodic boundary condition. In the first three subsections, we use $f(u)$ given by (36) with $\theta = 0.8$ and $\theta_c = 1.6$. The positive root γ of $f(\gamma) = 0$ is approximately $\gamma \approx 0.9575$. The energy functional corresponding to (38) is given by

$$E(u) = \int_{(0,1)^d} \left(\frac{\varepsilon^2}{2} |\nabla u(\boldsymbol{x})|^2 + F(u(\boldsymbol{x})) \right) \mathrm{d}\boldsymbol{x}, \tag{39}$$

where $F(u)$ is the Flory–Huggins potential (35). In the last subsection, we will adopt the monotonic source term $f(u)$ discussed in Example 3.4 and the related parameters will be given later.

In all experiments, we always adopt the five-point central difference matrix (32) or (34) to approximate the Laplace operator on the spatial uniform mesh with the size h given later. Since the approximating matrix is circulant, the product of the matrix exponential and a vector can be calculated via the fast Fourier transform. We mainly consider the 2D case and one 3D experiment will be conducted to compare the practical efficiency of the IFRK schemes.

4.1. Convergence tests

First, we test the convergence rates of the IFRK schemes (24), (26), (27), and (30). The initial data is set to be

$$u_0(x, y) = 0.1(\sin 3\pi x \sin 2\pi y + \sin 5\pi x \sin 5\pi y).$$

We use the spatial mesh size $h = 1/2048$. For the cases $\varepsilon = 0.1$ and $\varepsilon = 0.01$, we calculate the numerical solutions at $T = 2$ with the time step sizes $\tau = 2^{-k}$, $k = 1, 2, \ldots, 12$ and regard the solution obtained by IFRK4 with $\tau = 0.1 \times 2^{-12}$ as the benchmark to compute the supremum-norm errors. Fig. 1 shows the results of the convergence tests and the expected convergence rates are obvious. Moreover, we see that the accuracy of the IFRK4 scheme outperforms the lower-order schemes. For instance, the IFRK4 scheme with $\tau = 0.08$, around the upper bound determined by (31), yields the numerical errors around 10^{-7} (Fig. 1-(d)), while $\tau = 0.001$ is needed for the IFRK2 scheme reaching the same magnitude of the numerical errors (Fig. 1-(b)). In other words, given a requirement of accuracy, the IFRK4 scheme allows much larger time step sizes than the lower-order schemes, and thus, is less time-consuming and more efficient, which will be verified further in Section 4.3.

4.2. Tests for MBP preservation

To test the MBP-preserving property of the IFRK schemes, we simulate the process of the coarsening dynamics by setting $\varepsilon = 0.1$ and the spatial mesh size $h = 1/512$, where the initial data is given by random numbers on each mesh point ranging from -0.8 to 0.8.

We first use the IFRK schemes (24), (26), (27), and (30) with the uniform time step size $\tau = 0.08$, close to the upper bound of the time step sizes determined by (31) for the IFRK4 scheme. Fig. 2 plots the evolutions of the supremum norms of the numerical solutions. The red dash horizontal line shows the theoretical upper bound γ of the numerical solutions and the black solid curve gives a benchmark obtained by the IFRK4 scheme with $\tau = 0.001$. It can be observed that the supremum norms of the numerical solutions are always bounded by the theoretical value, and more precisely, the values of vertical coordinate of every curve do not exceed γ, which suggests the preservation of the MBP. In addition, the curves corresponding to the IF1 and IFRK2 schemes produce obvious deviations from the benchmark due to the low accuracy, while there is little difference between the curves for the IFRK3 and IFRK4 schemes and that for the benchmark. This shows the convergence of the four IFRK schemes and the benefit of high-order accurate schemes.

As we mentioned in Remark 3.2, the third-order IF Shu–Osher scheme (29) may not preserve the MBP due to the existence of the negative coefficient in the matrix exponential. Here, we simulate the coarsening dynamics described above using the scheme (29) with a small time step size $\tau = 0.005$ to explore the behavior of the numerical solution. The left

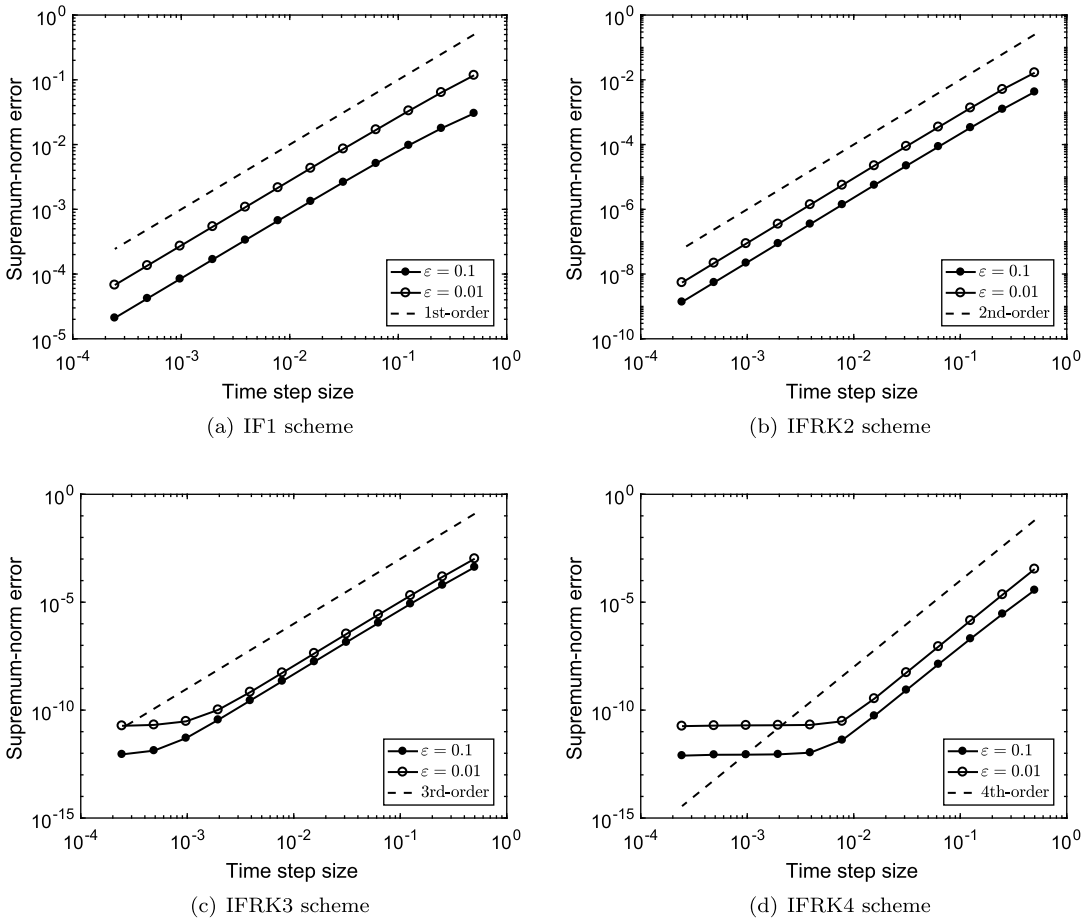

(a) IF1 scheme (b) IFRK2 scheme

(c) IFRK3 scheme (d) IFRK4 scheme

Fig. 1. Convergence rates of the IFRK schemes.

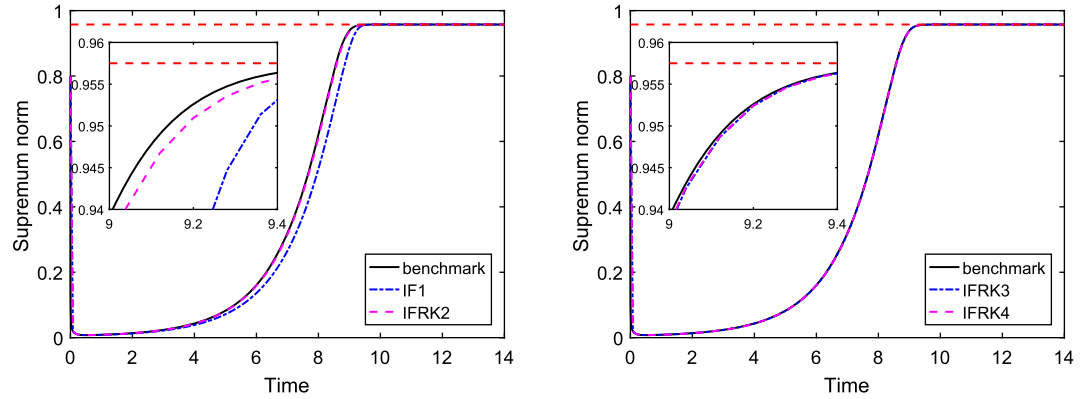

Fig. 2. Evolutions of the supremum norms of the solutions of IFRK schemes. (For interpretation of the colors in the figure(s), the reader is referred to the web version of this article.)

graph in Fig. 3 shows the evolution of the supremum norm till $t = 5$. We can see that the supremum norm of the numerical solution (the solid line) exceeds the theoretical upper bound (the dash line) around $t = 4.8$ and even evolves larger than 1 after $t = 4.9$. Note that there is a logarithmic term in the nonlinear part and it will be evaluated by complex numbers if u ranges out of the interval $(-1, 1)$. The right graph in Fig. 3 shows that the energy (39) decreases along the time until a wrong sharp corner arises around $t = 4.9$. We see that the simulation gives a completely wrong result even though a small time step size is adopted for the scheme (29), which suggests the necessity of the property of non-decreasing abscissas. Actually, we also repeat the experiment by a smaller time step size 0.004 and obtain the correct result similar to that shown in Fig. 2. Thus we guess that the scheme (29) with the time step size $\tau \leq 0.004$ could give the correct numerical

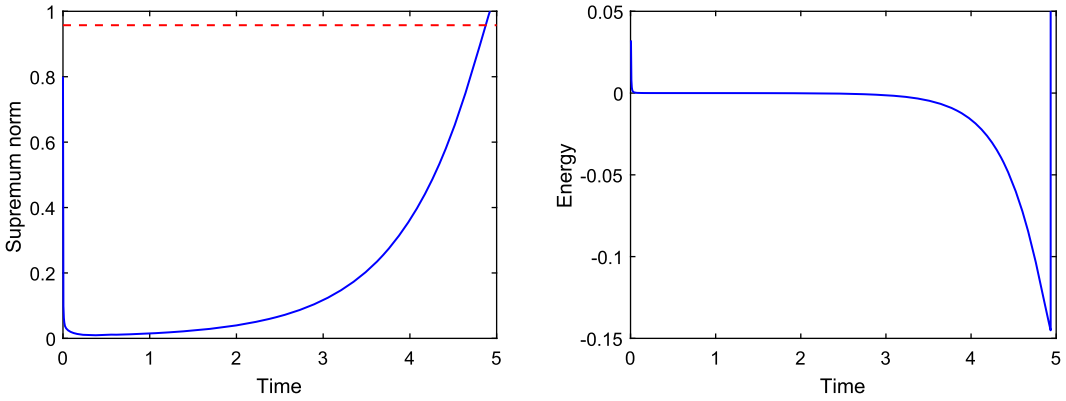

Fig. 3. Evolutions of the supremum norm (left) and the energy (right) of the solution of the third-order IF Shu–Osher scheme (29).

solutions. Moreover, according to the second inequality of (33), we further guess the scheme (29) may preserve the MBP when $\tau \le Ch^2$ for some constant C, though we do not have the theoretical proof.

4.3. Efficiency comparison for long-time 2D and 3D simulations

In this part, we aim to show the high efficiency of the IFRK4 scheme by simulating 2D and 3D coarsening dynamics in comparison with the lower-order schemes.

One may conclude from Fig. 1-(b) and (d) that the numerical error of the IFRK2 scheme with the time step size 0.001 has the same magnitude as the error of the IFRK4 scheme with the time step size about 0.08. Thus, we first conduct the simulation of the 2D coarsening dynamics with $\varepsilon = 0.01$ by adopting the IFRK2 scheme (26) with $\tau = 0.001$ and the IFRK4 scheme (30) with $\tau = 0.08$ to compare the efficiencies of these two schemes with the accuracy at the same level. The terminal time of the simulation is set to be $T = 610$.

The computations are carried out in MATLAB on a laptop with a four-core Intel 2.70 GHz Processor and 8 GB Memory. The CPU time for the computation by the IFRK2 scheme is about 5.87 hours and that for the IFRK4 scheme is around 13.96 minutes, approximately 3.96% of the former. This implies the higher efficiency of the IFRK4 scheme than that of the IFRK2 one. The numerical results of the IFRK4 scheme are shown in the following pictures (the results by the IFRK2 scheme are almost identical). Fig. 4 shows the configurations of the solution at $t = 4, 6, 10, 30, 100$, and 300. The simulated dynamics begins with a random state and towards the homogeneous steady state of constant $-\gamma$, which is reached after about $t = 600$ in our simulation. The evolutions of the supremum norm and the energy are plotted in Fig. 5. We observe that the energy decreases monotonically and the MBP is perfectly preserved so that the solution is always located in the interval $[-\gamma, \gamma]$.

Next, we simulate the 3D coarsening dynamics in the cube $\Omega = (0, 1)^3$ with $\varepsilon = 0.01$ and the random initial value ranging from -0.8 to 0.8 on the $128 \times 128 \times 128$ uniform spatial mesh. Again, we compare the elapsed times of the simulations using the IFRK4 scheme (30) with $\tau = 0.08$ and the IFRK2 scheme (26) with $\tau = 0.001$. The terminal time is set to be $T = 410$.

The computations are carried out in MATLAB on a desktop computer with an Intel 3.60 GHz Processor and 32 GB Memory. The CPU time for running the IFRK2 scheme is around 20.36 hours while that for the IFRK4 scheme is about 39.85 minutes. This again implies the high efficiency of the IFRK4 scheme, which is more obvious than the 2D case. Fig. 6 shows the evolution of the zero-isosurface of the numerical solution given by the IFRK4 scheme. Similar to the 2D case, the simulated dynamics begins with a random state and reaches the steady state of constant γ around $t = 407$. Fig. 7 plots the evolutions of the supremum norm and the energy, where the MBP is preserved and the energy decreases in time.

4.4. Simulation of the problem with a monotonic source

We close this section by considering the 2D problem (38) with $f(u) = a - e^u$ discussed in Example 3.4, which is not a typical gradient flow, thus we do not expect to see the phase separation as above. Setting $\varepsilon = 0.01$ and the spatial mesh size $h = 1/512$, we adopt the IFRK3 scheme (27) with suitable time step sizes to conduct the following experiments.

First, we consider the case $a \neq 1$. In particular, we set $a = 4$, then the bounding constant is $\ln 4 \approx 1.3863$. We set the time step size $\tau = 0.01$ satisfying (28) with (37), and the initial data is given by random numbers ranging from -0.8 to 0.8 on each mesh point. Fig. 8 shows the results of the simulation. We observe that the solution begins with reducing the noise in the initial state rapidly, and then evolves gradually to be flatter and closer to the steady state $u \equiv \ln 4$, reached around $t = 4$. The supremum norm of the solution is always smaller than the bounding constant, which means that the MBP is preserved as expected.

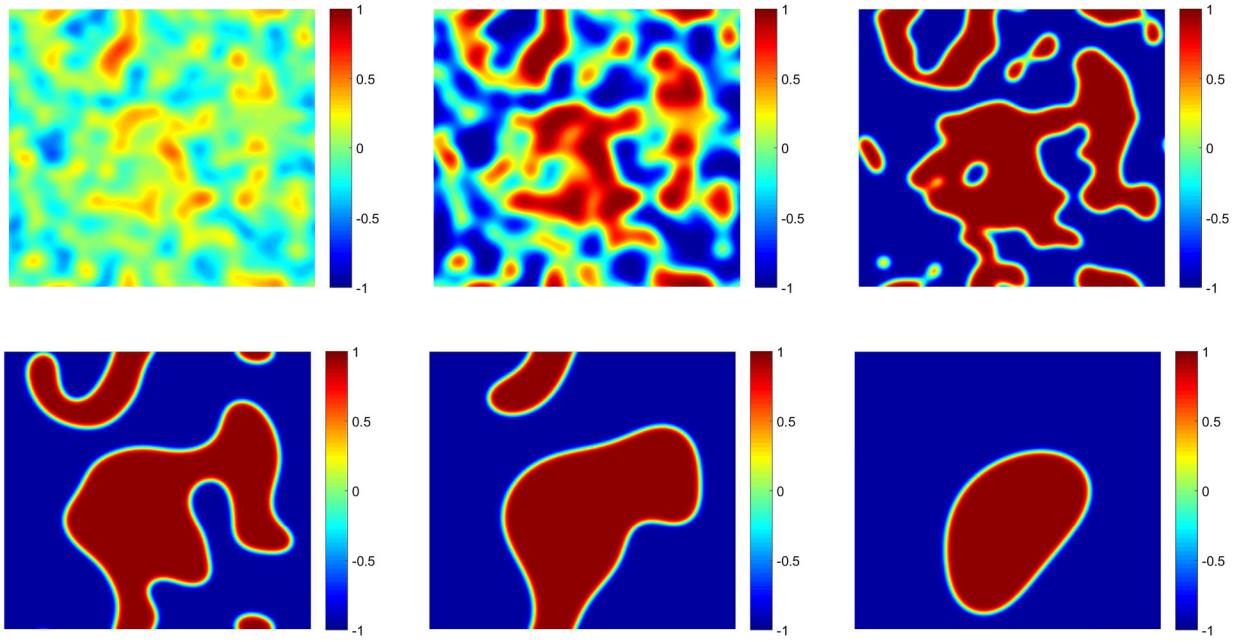

Fig. 4. The snapshots of the evolution at $t = 4, 6, 10, 30, 100, 300$, respectively (left to right and top to bottom), for the 2D coarsening dynamics.

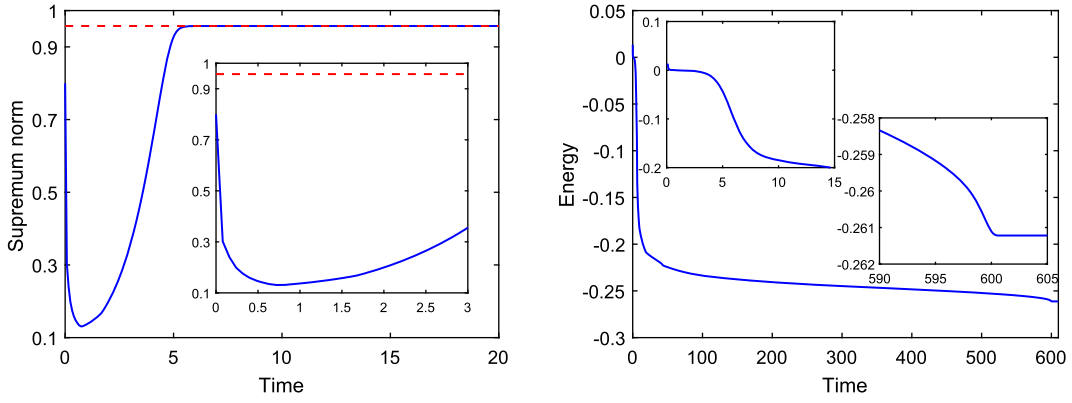

Fig. 5. Evolutions of the supremum norm (left) and the energy (right) for the 2D coarsening dynamics.

Then, by setting $a = 0.4$ with the bounding constant $|\ln 0.4| \approx 0.91629$, we carry out the simulation using the same initial state and time step size as above. We can see from Fig. 9 that the solution has a similar behavior as the previous case while it evolves to be smaller and smaller and reaches the negative constant $u \equiv \ln 0.4$ around $t = 30$. Again, the MBP is preserved perfectly.

Next, we consider the case $a = 1$, where the supremum norm of the solution to (38) is nonincreasing towards zero. To verify this numerically, we use the random numbers between $-\sigma$ and σ as the initial value, where $\sigma = 9, 0.1, 0.001, 0.00001$, respectively. To meet the requirement (28), we use $\tau = 0.001$ for the case $\sigma = 9$ and $\tau = 0.01$ for others. Fig. 10 plots the evolutions of the supremum norms using the semi-logarithm coordinates. Obviously, each curve decreases monotonically in time until the steady state $u \equiv 0$ is reached, which agrees with the discussion in Example 3.4; in other words, the MBP is preserved. (Actually, the computed values of the steady state are around 10^{-16} due to the machine error, so we drop off the part with values smaller than 10^{-15} in the graph.) In addition, we find that the decreasing rate of the supremum norm is exponential, which is consistent with the result in [4], where the long-time behavior of the solution was studied for (38) but with different type of boundary conditions.

5. Concluding remarks

In this work, we study the fully-discrete MBP-preserving IFRK method for a class of semilinear parabolic equations taking the form (1). We show that the IFRK method in general form preserves the MBP under certain conditions, present several

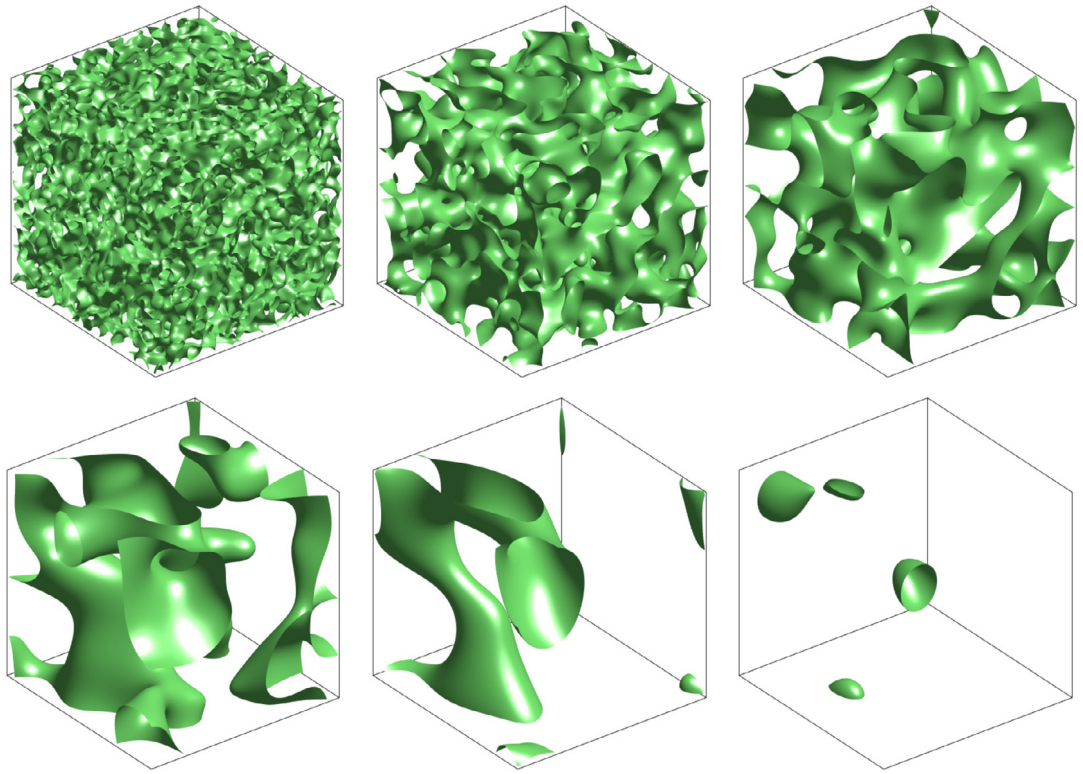

Fig. 6. The snapshots of the evolution at $t = 2, 10, 40, 100, 240, 370$, respectively (left to right and top to bottom), for the 3D coarsening dynamics.

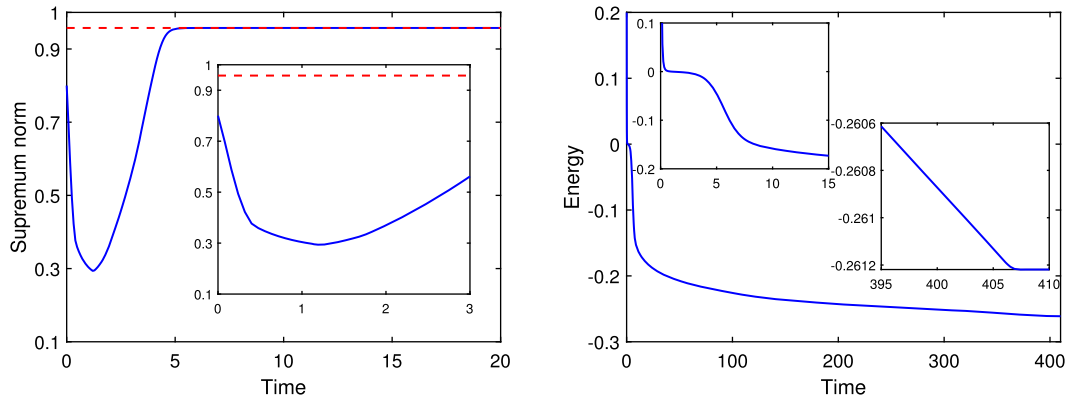

Fig. 7. Evolutions of the supremum norm (left) and the energy (right) for the 3D coarsening dynamics.

practical and specific IFRK schemes up to fourth order, and give the convergence analysis of these schemes. As shown in Theorem 3.1, the constraints on the time step size do not depend on the linear part, which is a significant advantage in comparison with the standard explicit SSP-RK methods where a CFL restriction is often needed. The four-stage IFRK4 scheme (30) provides a high-order MBP-preserving numerical scheme for the first time and its high efficiency was verified by the numerical simulation of 2D and 3D long-time evolutions.

There are some related problems worthy to explore further as continuation of this paper. On one hand, the IF1, IFRK2, and IFRK3 schemes presented in Section 3.3 actually come from the SSP-RK schemes in [20] for the system (8) with $L = 0$, while the IFRK4 scheme comes from the classic fourth-order RK method with the inevitable negative β_{ij}. Thanks to the conditions (10) and (11) for the nonlinear function, the nonnegativity constraint of β_{ij} is not necessary in our framework. Therefore, one of our future works is to explore whether it is possible to find a fifth-order (or even higher-order) MBP-preserving IFRK scheme by using similar routine as finding SSP schemes without the requirement of the nonnegativity of β_{ij}. On the other hand, the preservation of the MBP requires a constraint on the time step size due to the conditions (10) and (11). Thus, it is also expected to answer whether one can use the stabilizing technique, by adding a stabilization term as done in

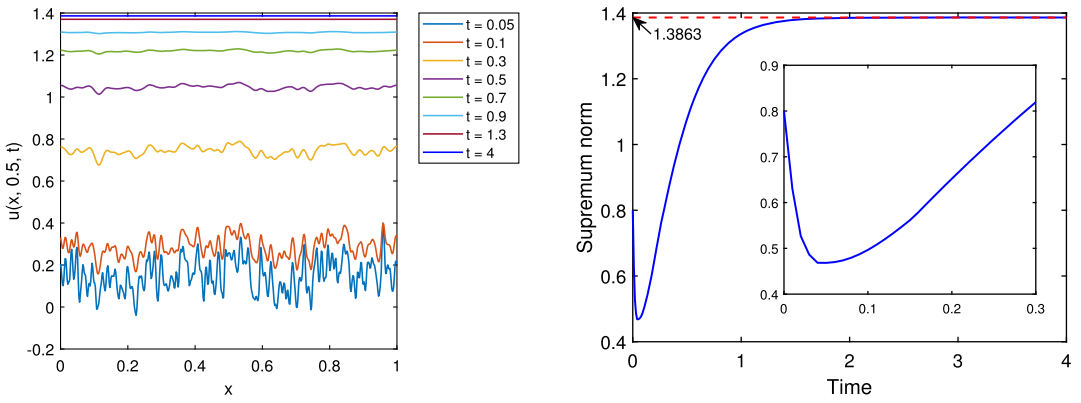

Fig. 8. Solution at different times (left) and evolution of the supremum norm (right) for the case $f(u) = 4 - e^u$.

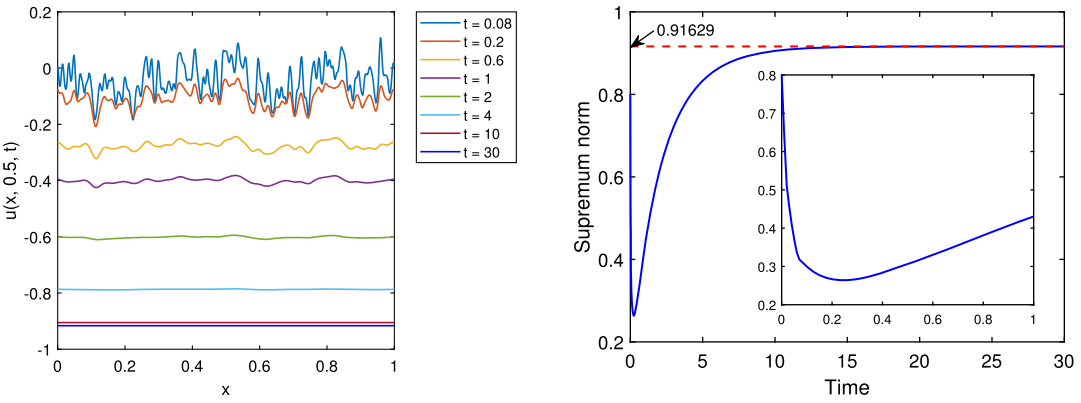

Fig. 9. Solution at different times (left) and evolution of the supremum norm (right) for the case $f(u) = 0.4 - e^u$.

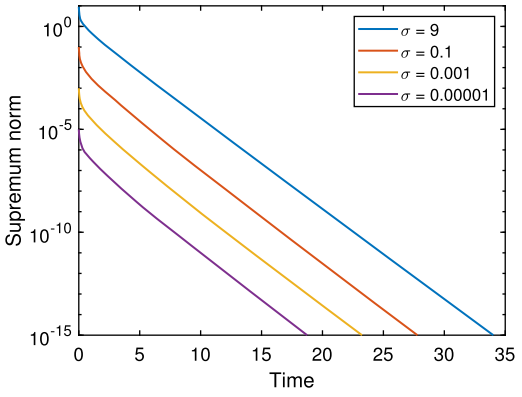

Fig. 10. Evolution of the supremum norm for the case $f(u) = 1 - e^u$.

[10,34], to remove the requirement on the time step size. In addition, the generalization to vector- and matrix-valued MBPs, including the complex Ginzburg–Landau model [8] and orthogonal matrix-valued equations [30] as the examples, can also be considered as done in [11].

CRediT authorship contribution statement

Lili Ju: Conceptualization, Methodology, Reviewing and Editing, Supervision; **Xiao Li:** Methodology, Software, Writing-Original draft preparation; **Zhonghua Qiao:** Conceptualization, Methodology, Reviewing and Editing, Supervision; **Jiang Yang:** Conceptualization, Methodology, Reviewing and Editing.

Declaration of competing interest

The authors declare that they have no known competing financial interests or personal relationships that could have appeared to influence the work reported in this paper.

Acknowledgements

We are grateful to Professor Chi-Wang Shu of Brown University for many valuable comments. This work is supported by the CAS AMSS-PolyU Joint Laboratory of Applied Mathematics. L. Ju's work is partially supported by US National Science Foundation grant DMS-1818438 and US Department of Energy grant DE-SC0020270. X. Li's work is partially supported by National Natural Science Foundation of China grant 11801024. Z. Qiao's work is partially supported by the Hong Kong Research Council GRF grants 15300417 and 15302919 and the Hong Kong Polytechnic University grant G-UAEY. J. Yang's work is supported by National Natural Science Foundation of China grant 11871264, Natural Science Foundation of Guangdong Province (2018A0303130123), and NSFC/Hong Kong RGC Joint Research Scheme (NFSC/RGC 11961160718).

References

[1] S. Ahmed, X.F. Liu, High order integration factor methods for systems with inhomogeneous boundary conditions, J. Comput. Appl. Math. 348 (2019) 89–102.
[2] S.M. Allen, J.W. Cahn, A microscopic theory for antiphase boundary motion and its application to antiphase domain coarsening, Acta Metall. 27 (1979) 1085–1095.
[3] G. Dahlquist, Stability and Error Bounds in the Numerical Integration of Ordinary Differential Equations, Trans. Royal Inst. of Technology, Stockholm, 1959, No. 130.
[4] K. Deng, Comparison principle for some nonlocal problems, Q. Appl. Math. 50 (1992) 517–522.
[5] Q. Du, Discrete gauge invariant approximations of a time-dependent Ginzburg–Landau model of superconductivity, Math. Comput. 67 (1998) 965–986.
[6] Q. Du, Numerical approximations of the Ginzburg–Landau models for superconductivity, J. Math. Phys. 46 (2005) 095109.
[7] Q. Du, M. Gunzburger, R.B. Lehoucq, K. Zhou, Analysis and approximation of nonlocal diffusion problems with volume constraints, SIAM Rev. 54 (2012) 667–696.
[8] Q. Du, M. Gunzburger, J. Peterson, Analysis and approximation of Ginzburg–Landau models for superconductivity, SIAM Rev. 34 (1992) 54–81.
[9] Q. Du, L. Ju, X. Li, Z.H. Qiao, Stabilized linear semi-implicit schemes for the nonlocal Cahn–Hilliard equation, J. Comput. Phys. 363 (2018) 39–54.
[10] Q. Du, L. Ju, X. Li, Z.H. Qiao, Maximum principle preserving exponential time differencing schemes for the nonlocal Allen–Cahn equation, SIAM J. Numer. Anal. 57 (2019) 875–898.
[11] Q. Du, L. Ju, X. Li, Z.H. Qiao, Maximum bound principles for a class of semilinear parabolic equations and exponential time differencing schemes, SIAM Rev. 63 (2021) 317–359.
[12] Q. Du, L. Ju, J.F. Lu, Analysis of fully discrete approximations for dissipative systems and application to time-dependent nonlocal diffusion problems, J. Sci. Comput. 78 (2019) 1438–1466.
[13] Q. Du, Y.Z. Tao, X.C. Tian, J. Yang, Asymptotically compatible discretization of multidimensional nonlocal diffusion models and approximation of nonlocal Green's functions, IMA J. Numer. Anal. 39 (2019) 607–625.
[14] Q. Du, J. Yang, Z. Zhou, Time-fractional Allen–Cahn equations: analysis and numerical methods, J. Sci. Comput. 85 (2020) 42.
[15] Q. Du, W.-X. Zhu, Analysis and applications of the exponential time differencing schemes and their contour integration modifications, BIT Numer. Math. 45 (2005) 307–328.
[16] L.C. Evans, H.M. Soner, P.E. Souganidis, Phase transitions and generalized motion by mean curvature, Commun. Pure Appl. Math. 45 (1992) 1097–1123.
[17] X.L. Feng, T. Tang, J. Yang, Stabilized Crank–Nicolson/Adams–Bashforth schemes for phase field models, East Asian J. Appl. Math. 3 (2013) 59–80.
[18] H.D. Gao, L. Ju, W. Xie, A stabilized semi-implicit Euler gauge-invariant method for the time-dependent Ginzburg–Landau equations, J. Sci. Comput. 80 (2019) 1083–1115.
[19] S. Gottlieb, C.-W. Shu, Total variation diminishing Runge–Kutta schemes, Math. Comput. 67 (1998) 73–85.
[20] S. Gottlieb, C.-W. Shu, E. Tadmor, Strong stability-preserving high-order time discretization methods, SIAM Rev. 43 (2001) 89–112.
[21] Z. Guan, C. Wang, S.M. Wise, A convergent convex splitting scheme for the periodic nonlocal Cahn–Hilliard equation, Numer. Math. 128 (2014) 377–406.
[22] E. Hairer, S.P. Norsett, G. Wanner, Solving Ordinary Differential Equations I: Nonstiff Problems, 2nd ed., Springer Ser. Comput. Math., vol. 8, Springer-Verlag, Berlin, 1993.
[23] T.L. Hou, H.T. Leng, Numerical analysis of a stabilized Crank–Nicolson/Adams–Bashforth finite difference scheme for Allen–Cahn equations, Appl. Math. Lett. 102 (2020) 106150.
[24] T.L. Hou, T. Tang, J. Yang, Numerical analysis of fully discretized Crank–Nicolson scheme for fractional-in-space Allen–Cahn equations, J. Sci. Comput. 72 (2017) 1214–1231.
[25] T.L. Hou, D.F. Xiu, W.Z. Jiang, A new second-order maximum-principle preserving finite difference scheme for Allen–Cahn equations with periodic boundary conditions, Appl. Math. Lett. 104 (2020) 106265.
[26] L. Isherwood, Z.J. Grant, S. Gottlieb, Strong stability preserving integrating factor Runge–Kutta methods, SIAM J. Numer. Anal. 56 (2018) 3276–3307.
[27] L. Ju, X. Li, Z.H. Qiao, H. Zhang, Energy stability and error estimates of exponential time differencing schemes for the epitaxial growth model without slope selection, Math. Comput. 87 (2018) 1859–1885.
[28] L. Ju, X.F. Liu, W. Leng, Compact implicit integration factor methods for a family of semilinear fourth-order parabolic equations, Discrete Contin. Dyn. Syst., Ser. B 19 (2014) 1667–1687.
[29] E. Nezza, G. Palatucci, E. Valdinoci, Hitchhiker's guide to the fractional Sobolev spaces, Bull. Sci. Math. 136 (2012) 521–573.
[30] B. Osting, D. Wang, A diffusion generated method for orthogonal matrix-valued fields, Math. Comput. 89 (2020) 515–550.
[31] D.Y. Peng, D.B. Robinson, A new two-constant equation of state, Ind. Eng. Chem. Fundam. 15 (1976) 59–64.
[32] Z.H. Qiao, S.Y. Sun, Two-phase fluid simulation using a diffuse interface model with Peng–Robinson equation of state, SIAM J. Sci. Comput. 36 (2014) B708–B728.
[33] Z.H. Qiao, Z.R. Zhang, T. Tang, An adaptive time-stepping strategy for the molecular beam epitaxy models, SIAM J. Sci. Comput. 33 (2011) 1395–1414.
[34] J. Shen, T. Tang, J. Yang, On the maximum principle preserving schemes for the generalized Allen–Cahn equation, Commun. Math. Sci. 14 (2016) 1517–1534.
[35] J. Shen, C. Wang, X.M. Wang, S.M. Wise, Second-order convex splitting schemes for gradient flows with Ehrlich–Schwoebel type energy: application to thin film epitaxy, SIAM J. Numer. Anal. 50 (2012) 105–125.

[36] J. Shen, J. Xu, J. Yang, A new class of efficient and robust energy stable schemes for gradient flows, SIAM Rev. 61 (2019) 474–506.
[37] J. Shen, X.F. Yang, Numerical approximations of Allen–Cahn and Cahn–Hilliard equations, Discrete Contin. Dyn. Syst. 28 (2010) 1669–1691.
[38] C.-W. Shu, S. Osher, Efficient implementation of essentially non-oscillatory shock-capturing schemes, J. Comput. Phys. 77 (1988) 439–471.
[39] G. Söderlind, The logarithmic norm. History and modern theory, BIT Numer. Math. 46 (2006) 631–652.
[40] P. Stehlík, J. Volek, Maximum principles for discrete and semidiscrete reaction-diffusion equation, Discrete Dyn. Nat. Soc. (2015) 791304.
[41] C. Ta, D.Y. Wang, Q. Nie, An integration factor method for stochastic and stiff reaction-diffusion systems, J. Comput. Phys. 295 (2015) 505–522.
[42] T. Tang, J. Yang, Implicit-explicit scheme for the Allen–Cahn equation preserves the maximum principle, J. Comput. Math. 34 (2016) 471–481.
[43] T. Tang, J. Yang, Framework of monotone schemes preserving the maximum principle for Allen–Cahn equations, preprint, 2019.
[44] W.Y. Tian, H. Zhou, W.H. Deng, A class of second order difference approximations for solving space fractional diffusion equations, Math. Comput. 84 (2015) 1703–1727.
[45] S.M. Wise, C. Wang, J.S. Lowengrub, An energy stable and convergent finite difference scheme for the phase field crystal equation, SIAM J. Numer. Anal. 47 (2009) 2269–2288.
[46] X.F. Xiao, X.L. Feng, J.Y. Yuan, The stabilized semi-implicit finite element method for the surface Allen–Cahn equation, Discrete Contin. Dyn. Syst., Ser. B 22 (2017) 2857–2877.
[47] C.J. Xu, T. Tang, Stability analysis of large time-stepping methods for epitaxial growth models, SIAM J. Numer. Anal. 44 (2006) 1759–1779.
[48] J. Yang, Q. Du, W. Zhang, Uniform L^p-bound of the Allen–Cahn equation and its numerical discretization, Int. J. Numer. Anal. Model. 18 (2018) 213–227.
[49] X.F. Yang, Linear, first and second-order, unconditionally energy stable numerical schemes for the phase field model of homopolymer blends, J. Comput. Phys. 327 (2016) 294–316.
[50] L.A. Ying, A second order explicit finite element scheme to multi-dimensional conservation laws and its convergence, Sci. China Ser. A 43 (2000) 945–957.